

# Microscopic Insights into the Sputtering of Ag{111} Induced by C<sub>60</sub> and Ga Bombardment

Zbigniew Postawa,<sup>\*,†</sup> Bartłomiej Czerwinski,<sup>†</sup> Marek Szewczyk,<sup>†</sup> Edward J. Smiley,<sup>‡,§</sup>  
Nicholas Winograd,<sup>‡,§</sup> and Barbara J. Garrison<sup>\*,‡</sup>

*Smoluchowski Institute of Physics, Jagiellonian University, Krakow, Poland, Department of Chemistry,  
152 Davey Laboratory, Penn State University, University Park, Pennsylvania 16802, and  
184 Materials Research Institute, Penn State University, University Park, Pennsylvania 16802*

*Received: January 6, 2004; In Final Form: March 22, 2004*

Molecular dynamics computer simulations have been utilized to compare the differences in the mechanism of sputtering of Ag{111} by kiloelectronvolt Ga and C<sub>60</sub> projectiles. The calculated kinetic energy distributions of Ag monomers and Ag<sub>2</sub> dimers compare favorably with experimental results. The damage caused by the C<sub>60</sub> particle left in the sample is less than the depth of material that the next impinging C<sub>60</sub> particle would remove, thus supporting the preliminary experimental observations that molecular depth profiling is possible with C<sub>60</sub> projectile beams.

## Introduction

There has been a recent flurry of interest in utilizing energetic buckminsterfullerene (C<sub>60</sub>) molecules<sup>1–12</sup> for surface characterization in time-of-flight secondary ion mass spectrometry (SIMS) experiments.<sup>13</sup> For these experiments, C<sub>60</sub><sup>+</sup> ions are accelerated to between 10 and 20 keV, pulsed, and focused onto a target causing desorption of atoms and molecules from the near-surface region.<sup>1–3</sup> Cluster ion beams have been of interest in these types of experiments for many years since it has been noticed that surface molecules are desorbed with greater efficiency than with corresponding atomic ion beams.<sup>14–27</sup> When C<sub>60</sub> strikes a surface, however, the subsequent energy dissipation processes give rise to several fascinating phenomena with significant scientific implications. Detailed studies are now possible since a stable, long-lived source of C<sub>60</sub><sup>+</sup> ions has recently been developed.<sup>1–3</sup> This source is particularly interesting since the ion beam may be focused to a probe size of the order of 1 μm, opening the possibility of greatly improved molecule-specific imaging experiments.

The important phenomena associated with C<sub>60</sub> impact events encompass a range of observables. First, neutral yield enhancements relative to atomic projectiles of order 10-fold have been reported from bombarded metal surfaces,<sup>7</sup> and enhancements of more than 10000-fold have been reported for ionized small peptide molecules with molecular weights of up to several thousand daltons.<sup>1,12</sup> Second, there appears to be much less damage remaining on the sample surface after bombardment.<sup>4,11</sup> This observation has led to depth-profiling experiments on polycrystalline multilayer stacks which exhibit very little interlayer mixing.<sup>4,11</sup> Third, the combination of high secondary yields with low damage creation opens the possibility of using C<sub>60</sub> ion beams to profile through molecular structures without significantly altering the chemical composition.<sup>6,20</sup> This modality, if properly exploited, could create a new paradigm in

materials characterization. Already, examples of profiling through polymer thin films and amino acid ice solutions have been reported.<sup>6</sup> Moreover, preliminary imaging experiments have been performed to study the surface composition of single biological cells.<sup>10</sup> Using the depth-profiling idea, it may be possible to acquire a three-dimensional picture of such objects.

The focus of this study is to acquire a fundamental understanding of the processes that give rise to the unique properties associated with C<sub>60</sub> bombardment. To achieve this goal, we have utilized molecular dynamics (MD) computer simulations, already extensively developed for atomic and simple cluster bombardment of a variety of targets, to address this problem. The work has emerged from earlier model calculations of 10–20 keV C<sub>60</sub> impact on graphite,<sup>28,29</sup> diamond,<sup>30</sup> and Ag{111}.<sup>31</sup> These studies all showed that the primary energy is deposited very near the sample surface and that desorption is accompanied by the formation of mesoscopic impact craters.

In this work, an appropriate model system is proposed whereby the behavior of atomic bombardment and C<sub>60</sub> bombardment can be quantitatively compared. Specifically, we address the issues of yield enhancement for both atom and cluster emission, sample damage to establish implications for depth-profiling experiments, and kinetic energy and angular distributions of ejected atoms and clusters. The latter calculations are important since experimental measurements are available for comparison purposes and these comparisons are essential for testing the efficacy of the model itself. The calculations are performed using Ag{111} as a target. It is anticipated, however, that the protocols reported here will be useful for examining more complex materials, especially those involving molecular overlayers, where the molecular mechanisms associated with the intriguing effects noted above can be revealed in detail.

## Model Details

The bombardment of a clean Ag{111} surface is modeled using molecular dynamics computer simulations since MD simulations provide an excellent representation of particle bombardment events.<sup>32,33</sup> The MD simulations allow calculation of experimentally observable properties such as yield, kinetic energy distributions, and angular distributions. Of special interest

\* Corresponding authors. (Z.P.) Phone: (4812) 632-4888 ext. 5626. E-mail: zp@castor.if.uj.edu.pl. (B.J.G.) Phone: (814) 863-2103. E-mail: bjg@psu.edu.

<sup>†</sup> Jagiellonian University.

<sup>‡</sup> Department of Chemistry, Penn State University.

<sup>§</sup> Materials Research Institute, Penn State University.

in this study is the damage in the substrate resulting from the  $C_{60}$  projectile bombardment. As discussed below, the damage is found to be localized near the impact point making it possible to contain the important events in a finite size system in the simulation. An extensive description of the MD scheme is available elsewhere.<sup>32,34</sup>

The forces among the atoms are described by a blend of empirical pairwise additive and many-body potential energy functions. The Ag–Ag interactions are described by the molecular dynamics/Monte Carlo corrected effective medium (MD/MC-CEM) potential for fcc metals.<sup>35</sup> The Ga–Ag interactions are described using the purely repulsive Molière pairwise additive potential. The adaptive intermolecular potential, AIREBO, developed by Stuart and co-workers is used to describe the C–C interactions.<sup>36</sup> This potential is based on the reactive empirical bond-order (REBO) potential developed by Brenner for hydrocarbon molecules.<sup>37,38</sup> The AIREBO potential yields a binding energy per atom in the relaxed  $C_{60}$  cluster of 7.2 eV, which compares well with the experimental value of 7.4 eV.<sup>39</sup> Finally, the interaction between C and Ag atoms is described by a Lennard-Jones potential using established parameters.<sup>40</sup>

Our model approximating the Ag{111} substrate consists of a finite microcrystallite containing 166 530 atoms arranged in 39 layers of 4270 atoms each. The sample size ( $175 \text{ \AA} \times 174.5 \text{ \AA} \times 89.7 \text{ \AA}$ ) was chosen to minimize edge effects on the dynamical events leading to ejection of particles. Projectiles of 5, 10, 15, and 20 keV  $C_{60}$ , 15 keV Ga, and 250 eV C are directed normal to the surface. In addition, 15 keV  $C_{60}$  bombardment was examined for off-normal incidence. In this case, the impact azimuth was selected to avoid principal channeling directions of the {111} surface. A total of 1000 trajectories was calculated for 250 eV C and 300 trajectories for 15 keV Ga, and 47, 81, 83, and 29 trajectories were sampled for  $C_{60}$  with 5, 10, 15, and 20 keV, respectively. As discussed previously,<sup>31</sup> the motion induced by  $C_{60}$  bombardment is mostly independent of the initial aiming point. Consequently, fewer trajectories need to be sampled to obtain reliable statistics. Each trajectory was initiated with a fresh sample with all atoms in their equilibrium minimum energy positions. The atoms in the target initially have zero velocity. The atoms in the  $C_{60}$  projectile initially have no velocity relative to the center of mass motion that is initially aimed toward the solid. The trajectory is terminated when the total energy of the most energetic particle remaining in the solid is 0.1 eV, where the binding energy of Ag is 2.95 eV. In addition, we have made six test calculations with a termination energy of 0.01 eV. The calculations ran longer, but no additional ejected particles were observed. The time of each trajectory ranges between 4 and 13 ps and depends on the type of primary projectile, its impact point, and the manner in which the energy distributes within the solid.

There are two aspects of the computational setup that require special care. First, large pressure waves<sup>31,41–46</sup> are generated by the  $C_{60}$  bombardment that could possibly cause artifacts if allowed to reflect from the boundaries of the sample. Briefly, for the boundary conditions, we put a stochastic region<sup>47,48</sup> at 0 K and a rigid layer on five sides of the crystal. Second, the definition of ejected species must be carefully examined due to the eruption of the material caused by the  $C_{60}$  impact, as shown in Figure 1. The treatments of both of these computational issues have been discussed in detail.<sup>31</sup>

The simulations cannot be performed for the tens of microseconds that it takes particles to reach the detector in the experiment.<sup>32</sup> Consequently, ejected clusters at the end of the simulation may have sufficient internally energy to unimolecu-

larly decay.<sup>49,50</sup> To minimize the influence of this phenomenon and maintain a tractable computer time, we have divided the simulation into two time regimes. The movements of all particles in the system were traced until 9.5 ps or until the calculation termination conditions have been satisfied. Subsequently, only the movements of sputtered particles were followed up to 500 ps. The calculations performed by Wucher and Garrison show that most of the ejected unstable silver clusters decompose into stable fragments on a time scale of several tens of picoseconds.<sup>49,50</sup> Therefore, we believe that the adopted time limit is sufficient to take into account the significant portion of these events. The unimolecular decomposition has a noticeable influence on all ejection characteristics. We see, for instance, that the partial sputtering yields for monomers, dimers, and trimers ejected by 15 keV  $C_{60}$  bombardment measured immediately after sputtering and at 500 ps are modified by 13, 25, and 6%, respectively. The kinetic and internal energy spectra are also influenced by this phenomenon. For example, the kinetic energy distribution of Ag monomers sputtered by 15 keV  $C_{60}$  bombardment of a Ag{111} surface at normal incidence exhibits a 25% increase in the low-energy portion of the spectrum from atoms that originate from cluster dissociation. As a result, the kinetic energy spectra are shifted toward a lower kinetic energy if fragmentation is included in the analysis. Consequently, all the spectra shown in the figures are calculated for ejected particles traveling for 500 ps.

## Results and Discussion

An intriguing experimental suggestion for the use of  $C_{60}$  projectile beams is for depth profiling.<sup>1,4–6,11</sup> Thus we start our discussion with a description of the nature of the damage created in the substrate due to the  $C_{60}$  projectile. The total yield of particles of various types, e.g., Ag,  $Ag_2$ , and  $Ag_3$ , as a function of incident angle is considered next. Finally the energy and angular distributions of the monomers and dimers are examined, and the energy distributions are compared to experimental ones for  $C_{60}$  and Ga bombardment.

**Damage.** Cross-sectional views of the temporal evolution of typical collision events leading to ejection of atoms due to 15 keV Ga and  $C_{60}$  bombardment are shown in Figure 1. It is obvious that the nature of the energy deposition process is very different for these two projectiles. The high-energy Ga projectile penetrates deeper into the crystal creating a damaged area that is cylindrical in shape. The  $C_{60}$  bombardment event creates a mesoscale crater with concomitant pressure wave into the solid.<sup>31,41–46</sup> As described by Yamada and co-workers for  $C_{60}$  bombardment on diamond,<sup>51</sup> the  $C_{60}$  projectile dissociates upon impact and most of the carbon atoms are backscattered into the vacuum. The impact leads to nearly simultaneous motion and high disorder in a relatively shallow volume of the crystal below the surface in a very short time. This dense, liquidlike region closes off open channels so that individual carbon atoms have difficulty penetrating deeply into the sample. Consequently, a significant amount of the projectile's energy is deposited close to the surface, leading to the emission of many particles. The motions due to the mesoscale impact of the entire  $C_{60}$  particle and the collisions induced by the individual C atoms have inherently different character and different time scales. These two components influence the yields and kinetic energy distributions.

To approximate the long time structure of the system, one trajectory at each energy was integrated to 29 ps so that the stochastic region could drain excess energy and cool the crystal. Cross-sectional views of typical craters formed at 29 ps after

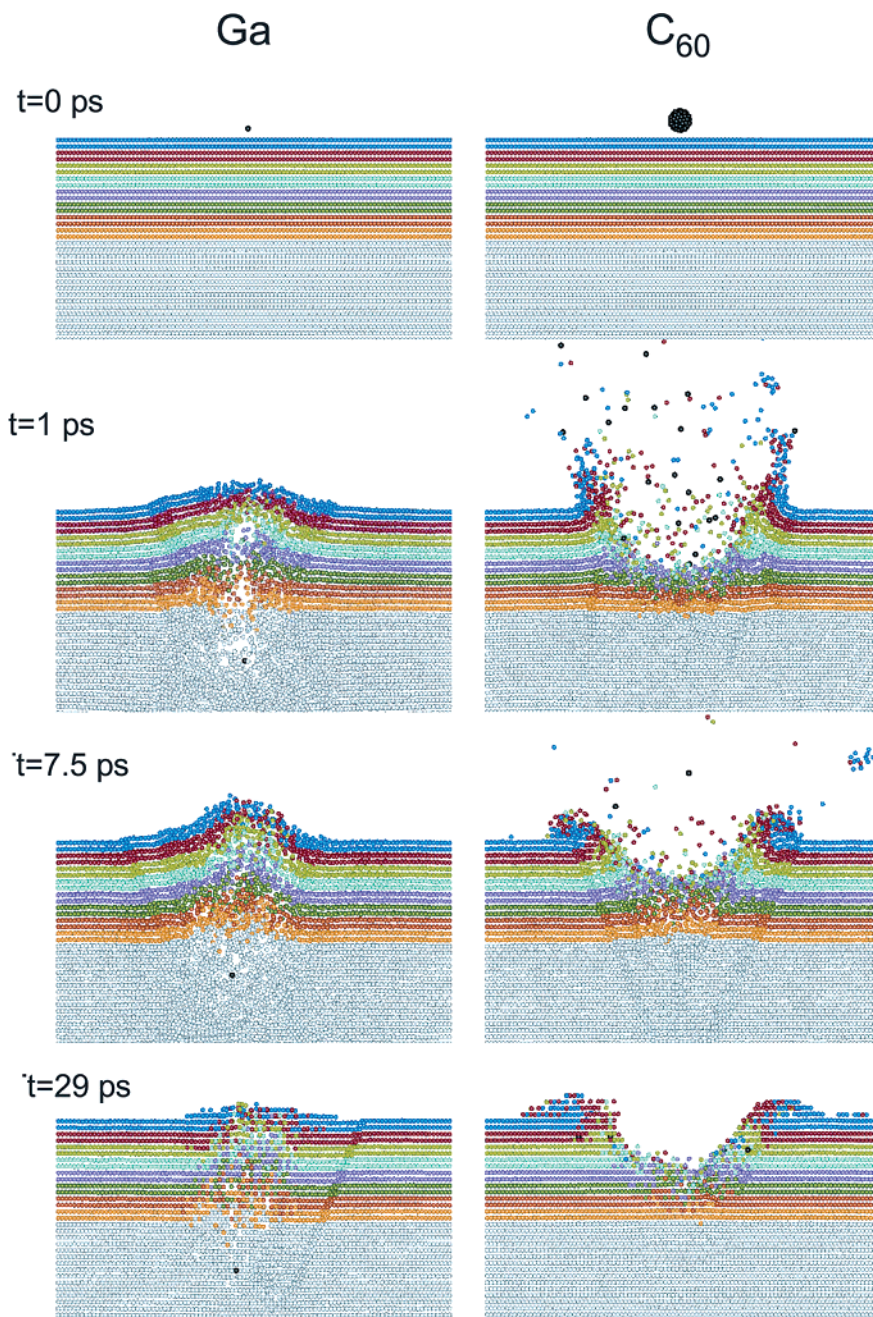


**Figure 1.** Cross-sectional view of the temporal evolution of a typical collision event leading to ejection of atoms due to 15 keV Ga and C<sub>60</sub> bombardment of a Ag{111} surface at normal incidence. The atoms are colored by original layers in the substrate. The projectile atoms are black.

C<sub>60</sub> impact are shown in Figure 2. As discussed previously,<sup>31,41–43</sup> the crater formation is almost mesoscopic in nature and only weakly depends on the initial impact point of the C<sub>60</sub> molecule on the surface. Thus, we feel that a detailed analysis of one trajectory gives the correct picture of the damage process. The crater has an almost circular shape surrounded by a rim. Each crater is surrounded by a region, the thickness of which increases with the kinetic energy of the projectile, where considerable atomic rearrangement or mixing occurs. Outside this region, the structure of the crystal is almost unaltered.

The crater size depends on the kinetic energy of the C<sub>60</sub> projectile. For the size estimate, the crater is assumed to be a half-ellipsoid with a radius  $R$  and a depth  $d$ . The estimated crater size and an approximate number of atoms that are missing from the crater,  $N_{\text{missing}}$ , are given in Table 1. The atoms were treated as missing if they were finally located at a distance  $a/4$  above the original surface plane, where  $a$  is the lattice constant. Both

the depth and radius of the crater were measured from four snapshots analogous to these presented in Figure 2. Table 1 shows that the crater volume increases with the projectile kinetic energy. The increase is greatest in the lateral dimension, i.e., diameter, rather than the depth of the crater. Over the range of experimental interest, 5–20 keV, however, the qualitative features of the mechanisms of particle removal and crater formation are independent of incident energy and incident angle (not shown). One would expect, therefore, to obtain similar qualitative results in the experiments, independent of the initial projectile energy.

The key aspect to depth-profiling experiments is a quantitative description of the spatial damage accumulated in the remaining material. We first examine the vertical rearrangements of atoms. The atoms considered are those in a cylinder of diameter 3 nm centered in the middle of the crater. For 5 keV bombardment, this dimension is slightly larger than the crater diameter but

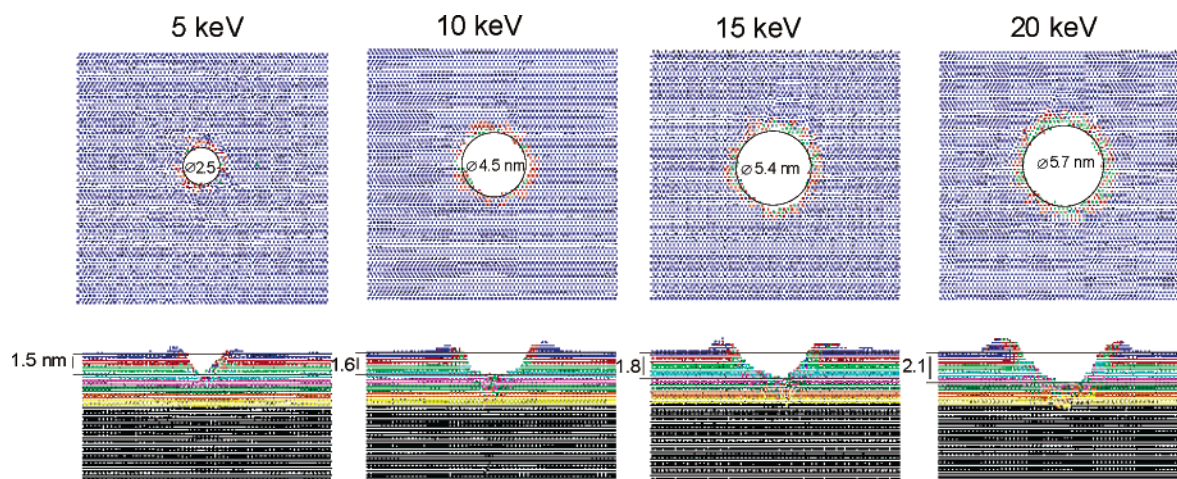


**Figure 2.** Cross-sectional top and side views of typical craters created by impact of the  $C_{60}$  projectile at the Ag{111} surface with various kinetic energies at a time of 29.5 ps. The top view shows only atoms that come to rest within  $\pm 0.5$  nm of the original surface plane. The crater diameter at the surface is given in each crater. The approximate depth of each crater is shown on the side view.

**TABLE 1: Crater Dimensions Estimated for Ag{111} Bombed with  $C_{60}$  Projectiles at Normal Incidence<sup>a</sup>**

| energy (keV) | depth (nm)     | radius (nm)     | $N_{\text{missing}}$ (Ag atoms) |
|--------------|----------------|-----------------|---------------------------------|
| 5            | $1.5 \pm 0.04$ | $1.25 \pm 0.14$ | $337 \pm 32$                    |
| 10           | $1.6 \pm 0.04$ | $2.25 \pm 0.14$ | $987 \pm 38$                    |
| 15           | $1.8 \pm 0.06$ | $2.70 \pm 0.09$ | $1590 \pm 72$                   |
| 20           | $2.1 \pm 0.05$ | $2.85 \pm 0.09$ | $2131 \pm 84$                   |

<sup>a</sup> The cratered depth, radius, and the number of removed atoms  $N_{\text{missing}}$  are given as a function of kinetic energy of a projectile. Each value is an average over four different bombardment events.

for the other energies, it is smaller than the top dimension of the crater. There are 220 atoms per layer considered in the analysis. The fraction of atoms sputtered, those that are relocated by more than a half-layer spacing in the vertical direction and those that are not relocated are given in Figure 3 as a function of layer number. All sputtered atoms arise from within the depth of the original crater. For the low energy of 5 keV, almost all of the atoms originate from the top two to three layers. The depth of origin of sputtered atoms increases with the increase of the kinetic energy of the  $C_{60}$  projectile. At the highest energy, 20 keV, even a few particles eject from as deep as the 9th or 10th layer. The relocated atoms are predominantly from one crater depth at the lowest energy to approximately twice that depth at the highest incident energy.

The horizontal damage is shown in Figure 4 for atoms that were originally in the top two layers of the crystal. The abscissa refers to the original distance of the atom in the crystal from the cylinder axis. The sputtered particles predominantly arise from distances of 1–3 nm from the impact point. The relocated particles arise from all regions but dominate directly under the impinging  $C_{60}$  projectile and at the edge of the crater as evident from Figure 2.

A qualitative assessment of the implications of  $C_{60}$  bombardment for depth profiling can be made by comparing the samples for the same amount of material removal. For atomic bombardment, the typical yield is on the order of tens of particles, e.g., the yield is 21 for 15 keV Ga bombardment of Ag as given in Table 2, whereas the analogous yield for  $C_{60}$  bombardment is 327. To obtain the same amount of material removal as with one  $C_{60}$  projectile, 10–20 Ga atoms must strike the same region of the target. As shown in Figure 1, the mixing of layers due to the Ga atom bombardment extends to 20 or more layers so that by the time the particles are being ejected from, for example, the 12th (orange) layer, the chemical identity is significantly

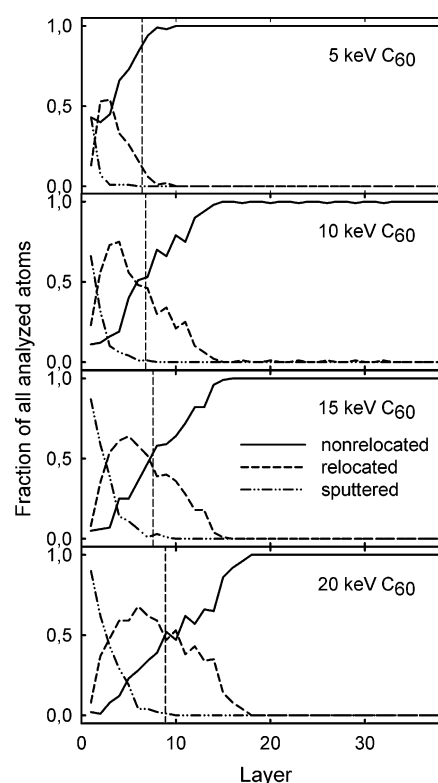


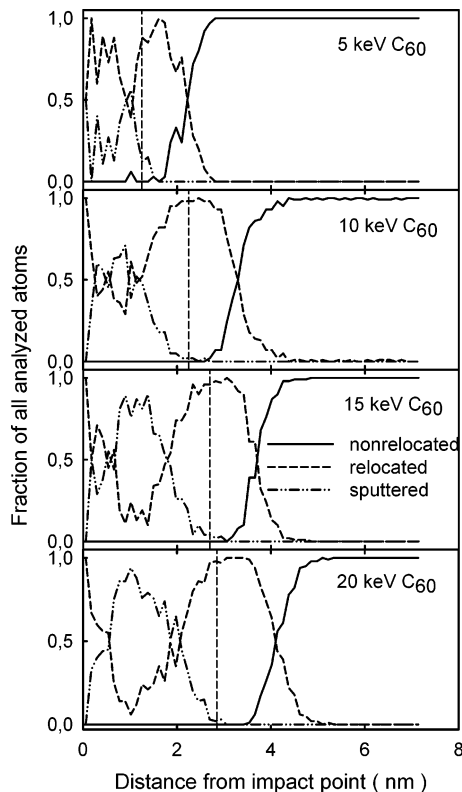
**Figure 3.** Vertical damage vs layer as a function of projectile incident energy. The layers are separated by 0.236 nm. Atoms are from a cylinder of diameter 3 nm or 220 atoms/layer. This size represents approximately the crater bottom for the 20 keV bombardment. The vertical line in each frame denotes the crater depth shown in Figure 2.

scrambled. The  $C_{60}$  bombardment, on the other hand, more efficiently removes the top layers of material, leaving the substrate less damaged.

Although the depth-profiling characteristics of  $C_{60}$  bombardment do not compete with the best of the low-energy beams designed for shallow depth profiling, there are some distinct attractive features. First, the  $C_{60}$  ion beam can be focused to a small spot,<sup>1,3</sup> allowing images to be recorded simultaneously with depth profiling. Second, the yield is larger than atomic beams; thus, the speed at which the sample erodes is faster. Third, since the mixed region is limited to a spatial area that occupies a smaller volume than the amount of material removed, it is conceivable that the next  $C_{60}$  impact will remove all of the

**TABLE 2: Total Sputtering Yield  $Y$  and a Number of Particles  $N$  Emitted from 5, 10, 15, and 20 keV C<sub>60</sub>, 15 keV Ga, and 250 eV C Bombarded Ag{111} Surface**

| projectile             | $Y$       | $N_{\text{tot}}$ | $N_{\text{Ag}}$ | $N_{\text{Ag}_2}$ | $N_{\text{Ag}_3}$ | $N_{\text{Ag}_4}$ |
|------------------------|-----------|------------------|-----------------|-------------------|-------------------|-------------------|
| 5 keV C <sub>60</sub>  | 49 ± 2    | 34 ± 1           | 23 ± 1          | 9 ± 1             | 2 ± 1             | 0.3 ± 0.1         |
| 10 keV C <sub>60</sub> | 174 ± 3   | 110 ± 2          | 70 ± 1          | 29 ± 1            | 7 ± 1             | 2 ± 0.1           |
| 15 keV C <sub>60</sub> | 327 ± 5   | 192 ± 2          | 115 ± 2         | 55 ± 1            | 12 ± 1            | 4 ± 0.2           |
| 20 keV C <sub>60</sub> | 482 ± 11  | 279 ± 5          | 171 ± 4         | 78 ± 2            | 17 ± 1            | 5 ± 0.4           |
| 250 eV C               | 1.9 ± 0.1 | 1.7 ± 0.1        | 1.6 ± 0.1       | 0.15 ± 0.01       | 0.01 ± 0.003      | <0.01             |
| 15 keV Ga              | 21 ± 2    | 18 ± 1           | 16 ± 1          | 2 ± 0.3           | 0.3 ± 0.05        | <0.1              |

**Figure 4.** Horizontal damage vs distance from the aiming point of the C<sub>60</sub> projectile as a function of projectile incident energy. Only atoms in the original top two layers of the crystal are considered with data collected in 0.28 nm annular rings. The vertical line in each frame denotes the crater width shown in Figure 2.

damaged region below the crater as well as pristine material. Hence, the computer simulations strongly suggest that there will be no damage buildup in the sample. The signal will always contain a significant component due to the unmixed and undamaged material. This situation should persist up to at least 20 keV incident kinetic energy.

**Sputtering Yield.** The difference in the sputtering yield resulting from atomic and cluster impacts is important in revealing whether there are nonlinear enhancement factors associated specifically with the cluster impact phenomenon. To test for this effect, the total and partial sputtering yields were calculated at 500 ps and are summarized in Table 2. The total sputtering yield for 15 keV C<sub>60</sub> (250 eV per individual C atom) bombardment is almost three times larger than the accumulated sputtering yield stimulated by 60 separate 250 eV carbon projectiles. Therefore, strong nonlinear effects indeed occur during C<sub>60</sub> impacts. Yield enhancements during cluster bombardment are well-known and have been observed both in calculations,<sup>41–43,52</sup> and in experiment.<sup>53–55</sup> In SIMS and positionization experiments, the total yield of material removed is generally not measured. Rather the average numbers of individual species such as monomers, dimers, and larger clusters are recorded. The average number of various ejected particles

is also shown in Table 2 to enable a more direct relationship of our data to the results obtained in experiment. The sputtering yields of all species increase with increasing energy of the primary particle.

The data in Table 2 show that proportionately more clusters eject for C<sub>60</sub> bombardment than either atomic Ga bombardment or atomic 250 eV C bombardment, indicating that emission of large clusters is favored during C<sub>60</sub> bombardment. Such behavior can be expected on the basis of the snapshots of the atomic motions shown in Figure 1. The development of a collision cascade immediately following impact exhibits a large density of energy deposited in subsurface volume by C<sub>60</sub> bombardment and large chunks of material are ejected at the early stages of development of the collision cascade. In addition, at later times a large number of slowly moving atoms enclosed near the base of the crater have the potential to favor more abundant cluster emission.

Measurements of the total amount of material sputtered from Ag due to C<sub>60</sub> bombardment are currently unavailable. A total removal yield resulting from 15 keV C<sub>60</sub> bombardment of polycrystalline gold at 45° incidence measured with a quartz crystal microbalance has been recently reported.<sup>56</sup> Since our objective is to determine if a factor of 15 in yield difference between atom and C<sub>60</sub> bombardment is plausible, we use this piece of experimental data. The experimental value of 200 Au particles removed per incident C<sub>60</sub> projectile agrees qualitatively with our predicted total yield of 218 for Ag under similar conditions shown in Table 3. Although the systems are not identical, Ag{111} under low-dose conditions vs polycrystalline Au under high-dose conditions, the comparison does show that the calculations give a sensible value for the total yield of particles removed.

The relation between the angle of incidence of the primary projectile and the total yield of sputtered particles can reflect important mechanistic details. Several of these calculations have been performed for C<sub>60</sub> bombardment, and the results are given in Table 3. The sputtering yield as well as the individual monomer, dimer, and trimer yields for 15 keV C<sub>60</sub> bombardment are found to decrease as the incident angle becomes more off-normal, except for possibly 15° incidence. This observation differs from the data reported for monatomic projectiles,<sup>57</sup> where the sputtering yield increases up to a certain critical angle, usually around 60°, and then starts to decrease. Such behavior for atomic bombardment has been attributed to the increase of the amount of projectile's kinetic energy deposited in the subsurface region with the increase of the impact angle. It is known that only this energy is responsible for ejection of particles.<sup>57</sup> Monatomic projectiles impinging at the surface at normal incidence deposit most of its kinetic energy at significant depth as shown for 15 keV Ga impact in Figure 1.

The sputtering initiated by C<sub>60</sub> bombardment on Ag{111} is qualitatively different. Most of the primary energy is deposited at the depth at which it can efficiently contribute to ejection. As a result, the ejection efficiency does not benefit from the increase of the impact angle. On the other hand, as the impact

**TABLE 3: Total Sputtering Yield  $Y$  and a Number of Particles  $N$  Emitted as a Function of Angle of Incidence for 15 keV  $C_{60}$  Bombardment**

| angle (deg) | $Y$          | $N_{tot}$   | $N_{Ag}$    | $N_{Ag2}$  | $N_{Ag3}$  | $N_{Ag4}$     |
|-------------|--------------|-------------|-------------|------------|------------|---------------|
| 0           | $327 \pm 6$  | $192 \pm 2$ | $115 \pm 1$ | $55 \pm 1$ | $12 \pm 1$ | $3.6 \pm 0.2$ |
| 15          | $336 \pm 9$  | $195 \pm 2$ | $116 \pm 2$ | $56 \pm 1$ | $12 \pm 1$ | $4.0 \pm 1.0$ |
| 30          | $275 \pm 12$ | $165 \pm 6$ | $106 \pm 6$ | $39 \pm 3$ | $11 \pm 1$ | $2.8 \pm 0.4$ |
| 45          | $218 \pm 6$  | $136 \pm 3$ | $88 \pm 2$  | $35 \pm 1$ | $8 \pm 1$  | $2.7 \pm 0.2$ |
| 60          | $90 \pm 6$   | $58 \pm 4$  | $36 \pm 4$  | $17 \pm 1$ | $3 \pm 1$  | $1.3 \pm 0.3$ |

angle increases, more energy is reflected into the vacuum, although the number of back-reflected carbon atoms remains almost the same. For example, for 15 keV  $C_{60}$  bombardment the average amount of kinetic energy carried away by reflected C atoms increases monotonically from 2 keV at normal incidence to 8.5 keV for 60° impact.

The mechanistic reason for the larger yield at normal bombardment rather than oblique bombardment hinges on the relatively large mass of the substrate compared to the impinging C atoms. The heavy Ag particles can easily reflect the light C atoms. Much of the interest in the SIMS community, however, is the use of  $C_{60}$  bombardment of Si for applications in the semiconductor industry or of organic and biological samples for mass spectrometric analysis and imaging. In both of the latter applications, the mass of the substrate matches more closely that of C and thus as much energy may not be carried off by the incident atoms. The implications of this angle dependence are not yet fully known. Experimental studies of  $C_{60}$  bombardment of silicon at various angles indicate that off-normal bombardment is more effective than normal bombardment.<sup>3</sup>

**Kinetic Energy and Angular Spectra.** The kinetic energy and angular spectra are briefly presented here in order to give a complete description of the differences in emission due to Ga and  $C_{60}$  bombardment. A full interpretation of the trends and shifts in peak positions is currently under study and will be given in a more specialized publication.<sup>58</sup> These comparisons are important because the predictions of the model are amenable for experimental measurement; thus, they give a means of validating the simulations.

Peak-normalized kinetic energy distributions of silver atoms sputtered by  $C_{60}$  and Ga and C projectiles are shown in Figure 5. The kinetic energy spectrum for 15 keV bombardment at 45° incidence is not shown since it looks very similar to the 10 and 20 keV  $C_{60}$  data. Only a small shift to lower kinetic energy is visible with the increase of the kinetic energy of the  $C_{60}$  projectile. On the other hand, the kinetic energy spectra of particles ejected with 15 keV Ga, 0.25 C, and 5 keV  $C_{60}$  projectiles peak at larger kinetic energy. As discussed above, there is interplay between the mesoscopic crater formation and the motion induced by the dissociated  $C_{60}$  cluster. The crater formation process tends to eject particles at higher kinetic energies, and the motion induced by the individual C atoms tends to give rise to slower moving particles. The 5 keV  $C_{60}$  distribution appears to be dominated by the higher energy ejection mechanism, the crater formation process, and appears similar to the atomic bombardment energy distributions. For the 10–20 keV  $C_{60}$  bombardment, the lower energy ejection process dominates and the peak in the distribution shifts to lower energies. It is known that the kinetic energy distribution of atoms ejected from a nonlinear regime peaks at a much lower kinetic energy than for atoms ejected from a linear collision cascade.<sup>59</sup>

The calculated and experimental<sup>7</sup> kinetic energy distributions of Ag monomers and dimers ejected by 15 keV Ga and  $C_{60}$  projectiles are shown in Figure 6. Measurements performed for atomic projectile bombardment indicate that the clusters are ejected with lower kinetic energies than the corresponding

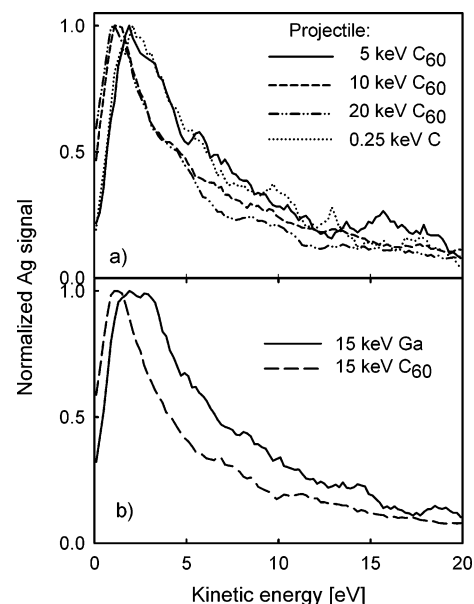


**Figure 5.** Peak-normalized kinetic energy distributions of silver atoms sputtered at normal incidence from Ag{111}: (a) C and  $C_{60}$  projectiles of various kinetic energy; (b) 15 keV Ga and  $C_{60}$  projectiles.

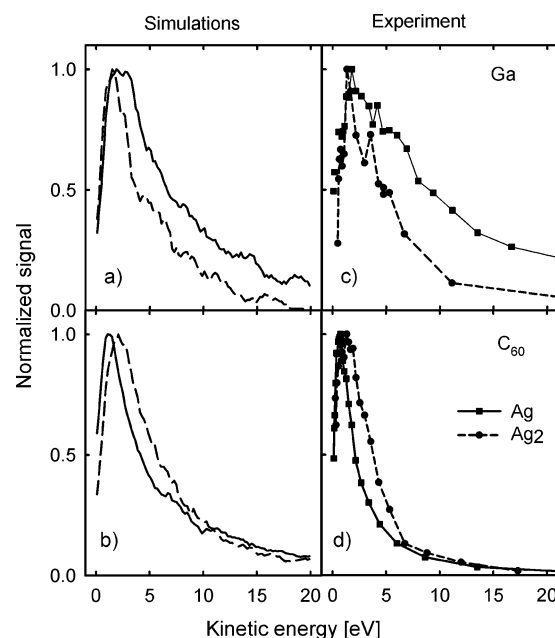


**Figure 6.** Theoretical and experimental kinetic energy distributions of silver monomers (solid line) and dimers (dashed line) sputtered by 15 keV  $C_{60}$  and Ga projectiles at normal incidence.

atomic species,<sup>60–62</sup> as shown in Figure 6 for Ga bombardment. In addition, it has been observed that the high-energy portion of the spectrum drops off faster than for atomic ejection. As shown in Figure 6, the behavior of  $Ag_2$  clusters ejected during Ga bombardment follows these trends. Ejection of silver dimers from the  $C_{60}$ -bombarded Ag{111} surface, however, does not follow these expectations. The dimers have, on average, larger

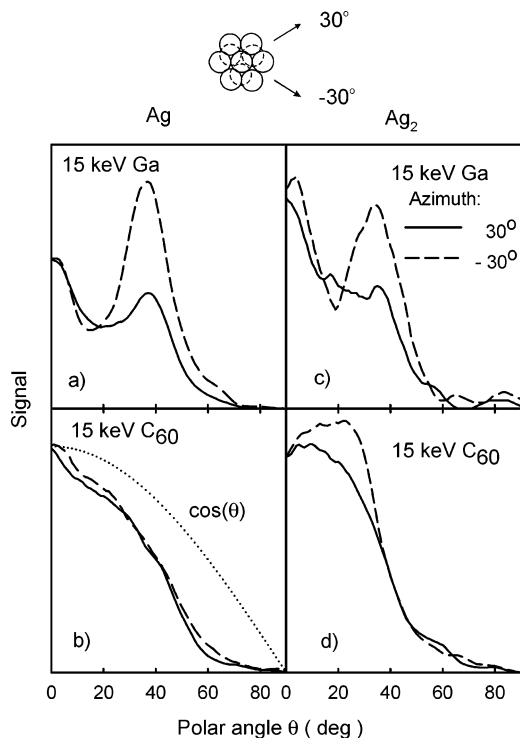


**Figure 7.** Angular distributions of silver atoms and dimers ejected from Ag{111} by 15 keV Ga and C<sub>60</sub> bombardment at normal incidence along +30° and -30° azimuths. Dotted lines indicate cos( $\theta$ ) dependence. The azimuthal directions are shown on a schematic of the surface where surface atoms are depicted as circles with solid lines and second layer atoms are depicted as circles with dashed lines.

kinetic energy than ejected Ag atoms in both the measured and calculated energy distributions. As mentioned above, there are two stages of emission of particles including dimers. The details of how these two mechanisms quantitatively contribute to the calculated and measured kinetic energy distribution are under further study.<sup>58</sup> The main point in this discussion is that the relative peak positions of the Ag and Ag<sub>2</sub> distributions shift due to C<sub>60</sub> vs Ga bombardment and that these trends are observed in both the experimental and calculated results.

The angular distributions of silver atoms and dimers ejected along -30 and +30 azimuths during 15 keV Ga and C<sub>60</sub> bombardment of Ag{111} are shown in Figure 7. Silver atoms and dimers ejected from the sample bombarded with 15 keV Ga exhibit well-known anisotropies, which are attributed to channeling and blocking.<sup>62</sup> On the other hand, almost no azimuthal anisotropy is visible for atoms and dimers ejected by C<sub>60</sub> bombardment, where most of the particles eject along the normal to the surface. The angular spectrum of emitted silver atoms, however, cannot be described by a cosine law, which would be expected if the atoms were simply evaporating from the surface. There are just a few measurements of angular distributions of particles ejected under nonlinear sputtering conditions. Toyoda et al. reported that copper particles are emitted predominantly at off-normal directions during bombardment of copper with an Ar<sub>3000</sub> cluster.<sup>63</sup> The authors propose that such a distribution is caused by a significant contribution of particles ejected from around that edge of the crater which obtain a high lateral momentum. Indeed, Colla and Urbassek also observed in their simulations that slow evaporation of clusters from the crater rim contributes mainly to the emission at angles close to the surface.<sup>42</sup> An almost cosine-like spectrum, however, was obtained if all particles were included in analysis. Observations from experiments of Toyoda et al.,<sup>63</sup> however,

cannot be directly compared to our simulations. Ejecting copper atoms on their way out have to penetrate through the huge Ar cluster, which will reduce the number of particles emitted in the normal direction. The angular spectra during small cluster bombardment have been measured by Andersen et al.<sup>55</sup> They found that angular distributions of material sputtered by cluster irradiation are more isotropic than distributions induced by monomer bombardment at the same velocity. This result agrees qualitatively with our observations.

As for the case of energy distributions, the angular distribution of the Ag<sub>2</sub> particles is also different when compared to atom emission. While monomers are predominantly ejected along the normal to the surface, most of the dimers are ejected at ~20° with respect to the normal direction. A full explanation of the mechanistic reasons for this angular dependence is under investigation.<sup>58</sup>

## Conclusions

The molecular dynamics simulations presented here establish the foundation and protocol for further studies of bombardment of kiloelectronvolt C<sub>60</sub> particles. The calculated kinetic energy distribution of Ag<sub>2</sub> dimers is narrower than the Ag monomer distribution for Ga bombardment but is broader for C<sub>60</sub> bombardment in agreement with experiment.<sup>7</sup> The calculations present a graphic illustration of the essential differences in C<sub>60</sub> bombardment vs atomic bombardment vis-à-vis the damage left in the remaining sample. The damage caused by the C<sub>60</sub> particle left in the sample is less than the depth of material that the next impinging C<sub>60</sub> particle would remove, thus supporting the preliminary experimental observations that molecular depth profiling is possible with C<sub>60</sub> projectile beams. The next obvious steps are to verify these observations for molecular thin films on metal substrates and to scale-up the simulations for organic solids.

**Acknowledgment.** The financial support from the Polish Committee for Scientific Research (Grant No. 3T09A12426), the CYFRONET Rector of Jagiellonian University, the National Science Foundation, and the National Institutes of Health is gratefully acknowledged. The Academic Services and Emerging Technologies group at Penn State provided us early access to the lion-xl PC cluster. We appreciate helpful discussions with Shixin Sun, Christopher Szakal, John Vickerman, and Andreas Wucher as well as access to their unpublished experimental data.

## References and Notes

- (1) Weibel, D.; Wong, S. C. C.; Lockyer, N.; Blenkinsopp, P.; Hill R.; Vickerman, J. C. *Anal. Chem.* **2003**, *75*, 1754.
- (2) Wong, S. C. C.; Hill, R.; Blenkinsopp, P.; Lockyer, N. P.; Weibel, D. E.; Vickerman, J. C. *Appl. Surf. Sci.* **2003**, *203–204*, 219.
- (3) Hill, R.; Blenkinsopp, P. W. M. The Development of C<sub>60</sub> and Gold Cluster Ion Guns for Static SIMS Analysis. *Appl. Surf. Sci.*, in press.
- (4) Sostarecz, A.; Sun, S.; Szakal, C.; Wucher, A.; Winograd, N. Depth Profiling Studies of Multilayer Films with a C<sub>60</sub><sup>+</sup> Ion Source. *Appl. Surf. Sci.*, in press.
- (5) Szakal, C.; Sun, S.; Wucher, A.; Winograd, N. C<sub>60</sub> Molecular Depth Profiling of a Model Polymer. *Appl. Surf. Sci.*, in press.
- (6) Wucher, A.; Sun, S.; Szakal, C.; Winograd, N. Molecular Depth Profiling in Ice Matrices Using C<sub>60</sub> Projectiles. *Appl. Surf. Sci.*, in press.
- (7) Sun, S.; Szakal, C.; Smiley, E. J.; Postawa, Z.; Wucher, A.; Garrison, B. J.; Winograd, N. Sputtering of Ag under C<sub>60</sub><sup>+</sup> and Ga<sup>+</sup> Projectile Bombardment. *Appl. Surf. Sci.*, in press.
- (8) Xu, J.; Ostrowski, S.; Ewing, A. G.; Winograd, N. ToF-SIMS Imaging with Cluster Beams. *Appl. Surf. Sci.*, in press.
- (9) Weibel, D. E.; Lockyer, N.; Vickerman, J. C. C<sub>60</sub> Cluster Ion Bombardment of Organic Surfaces. *Appl. Surf. Sci.*, in press.
- (10) Winograd, N. ToF Imaging with Cluster Ion Beams. *Appl. Surf. Sci.*, in press.

- (11) Sun, S.; Wucher, A.; Szakal, C.; Winograd, N. Depth Profiling of Polycrystalline Multilayers Using a Buckminsterfullerene Projectile. *Appl. Phys. Lett.*, submitted for publication.
- (12) Xu, J.; Szakal, C.; Martin, S. E.; Peterson, B. R.; Wucher, A.; Winograd, N. Molecule-Specific Imaging with Mass Spectrometry and a Buckminsterfullerene Probe: Application to Characterizing Solid-Phase Synthesized Combinatorial Libraries. *J. Am. Chem. Soc.*, in press.
- (13) *ToF-SIMS: Surface Analysis by Mass Spectrometry*; Vickerman, J. C., Briggs, D., Eds.; Della-Negra, S.; Joret, H.; Le Beyec, Y.; Schweikert, E. A. *Phys. Rev. Lett.* **1989**, *63*, 1625.
- (14) Castner, D. G. *Nature* **2003**, *422*, 122.
- (15) Applehans, A. D.; Delmore, J. E. *Anal. Chem.* **1989**, *61*, 1087.
- (16) Blain, M. G.; Della-Negra, S.; Joret, H.; Le Beyec, Y.; Schweikert, E. A. *Phys. Rev. Lett.* **1989**, *63*, 1625.
- (17) Van Stipdonk, M. J.; Harris, R. D.; Schweikert, E. A. *Rapid Commun. Mass Spectrom.* **1996**, *10*, 1987.
- (18) Takeuchi, D.; Seki, T.; Aoki, T.; Matsuo, J.; Yamada, I. *Mater. Chem. Phys.* **1998**, *54*, 76.
- (19) Mahoney, J. F.; Perel, J.; Ruatta, S. A.; Martine, P. A.; Husain, S.; Lee, T. D. *Rapid Commun. Mass Spectrom.* **1991**, *5*, 441.
- (20) Gillen, G.; Roberson, S. *Rapid. Commun. Mass Spectrom.* **1998**, *12*, 1303.
- (21) Gillen, G.; King, L.; Freibaum, B.; Lareau, R.; Bennett, J.; Chmara, F. *J. Vac. Sci. Technol., A* **2001**, *19*, 568.
- (22) Fuoco, E. R.; Gillen, G.; Wijesundara, M. B. J.; Wallace, W. E.; Hanley, L. *J. Phys. Chem. B* **2001**, *105*, 3950.
- (23) Kötter, F.; Benninghoven, A. *Appl. Surf. Sci.* **1998**, *133*, 47.
- (24) Prewett, P. D.; Jefferies, D. K. *J. Phys. D: Appl. Phys.* **1980**, *13*, 1747.
- (25) Hagenhoff, B.; Kersting, R.; Rading, D.; Kayser, S.; Niehuis, E. In *Proceedings of the 12th International Conference on Secondary Ion Mass Spectrometry*; Benninghoven, A., Bertrand, P., Migeon, H.-N., Werner, H. W., Eds.; 2000; p 833.
- (26) Davies, N.; Weibel, D. E.; Blenkinsopp, P.; Lockyer, N.; Hill, R.; Vickerman, J. C. *Appl. Surf. Sci.* **2003**, *203–204*, 223.
- (27) Walker, A. V.; Winograd, N. *Appl. Surf. Sci.* **2003**, *203–204*, 198.
- (28) Webb, R. P.; Kerford, M.; Way, A.; Wilson, I. *Nucl. Instrum. Methods B* **1999**, *153*, 284.
- (29) Seki, T.; Aoki, T.; Tanomura, M.; Matsuo, J.; Yamada, I. *Mater. Chem. Phys.* **1998**, *54*, 143.
- (30) Aoki, T.; Seki, T.; Matsuo, J.; Insepov, Z.; Yamada, I. *Mater. Chem. Phys.* **1998**, *54*, 139.
- (31) Postawa, Z.; Czerwinski, B.; Szewczyk, M.; Smiley, E.; Winograd, N.; Garrison, B. J. *Anal. Chem.* **2003**, *75*, 4402.
- (32) Garrison, B. J. In *ToF-SIMS: Surface Analysis by Mass Spectrometry*; Vickerman, J. C., Briggs, D., Eds.; SurfaceSpectra Ltd. & IMPublications: Manchester and Chichester, U.K., 2001; p 223.
- (33) Garrison, B. J.; Delcorte, A.; Krantzman, K. D. *Acc. Chem. Res.* **2000**, *33*, 69.
- (34) Garrison, B. J. *Chem. Soc. Rev.* **1992**, *21*, 155.
- (35) Kelchner, C. L.; Halstead, D. M.; Perkins, L. S.; Wallace, N. M.; DePristo, A. E. *Surf. Sci.* **1994**, *310*, 425.
- (36) Stuart, S. J.; Tutein, A. B.; Harrison, J. A. *J. Chem. Phys.* **2000**, *112*, 6472.
- (37) Brenner, D. W. *Phys. Rev. B* **1990**, *42*, 9458.
- (38) Brenner, D. W.; Shenderova, O. A.; Harrison, J. A.; Stuart, S. J.; Ni, B.; Sinnott, S. B. *J. Phys.: Condens. Matter* **2002**, *14*, 783.
- (39) <http://www.sesres.com/PhysicalProperties.asp>.
- (40) Postawa, Z.; Piaskowy, J.; Ludwig, K.; Winograd, N.; Garrison, B. J. *Nucl. Instrum. Methods* **2003**, *202*, 168.
- (41) Colla, Th. J.; Aderjan, R.; Kissel, R.; Urbassek, H. M. *Phys. Rev. B* **2000**, *62*, 8487.
- (42) Colla, Th. J.; Urbassek, H. M. *Nucl. Instrum. Methods B* **2000**, *164*, 687.
- (43) Aderjan, R.; Urbassek, H. M. *Nucl. Instrum. Methods B* **2000**, *164*, 697.
- (44) Webb, R. P.; Kerford, M. *Nucl. Instrum. Methods B* **2001**, *180*, 32.
- (45) Kerford, M.; Webb, R. P. *Nucl. Instrum. Methods B* **2001**, *180*, 44.
- (46) Haberland, H.; Isepov, Z.; Moseler, M. *Phys. Rev. B* **1995**, *51*, 11061.
- (47) Adelman, S. A.; Doll, J. D. *J. Chem. Phys.* **1974**, *61*, 4242.
- (48) Garrison, B. J.; Kodali, P. B. S.; Srivastava, D. *Chem. Rev.* **1996**, *96*, 1327.
- (49) Wucher, A.; Garrison, B. J. *Phys. Rev. B* **1992**, *46*, 4855.
- (50) Wucher, A.; Garrison, B. J. *J. Chem. Phys.* **1996**, *105*, 5999.
- (51) Aoki, T.; Seki, T.; Matsuo, J.; Insepov, Z.; Yamada, I. *Mater. Chem. Phys.* **1998**, *54*, 139.
- (52) Betz, G.; Husinsky, W. *Nucl. Instrum. Methods B* **1997**, *122*, 311.
- (53) Heinrich, R.; Wucher, A. In *Atomic Collisions in Solids*; Ellegard, O., Møller, S. P., Schou, J., Sigmund, P., Eds.; Elsevier Science: Amsterdam, 2000; p 720.
- (54) Andersen, H. H.; Bay, H. L. *J. Appl. Phys.* **1974**, *45*, 953; **1975**, *46*, 2416.
- (55) Andersen, H. H.; Brunelle, A.; Della-Negra, S.; Depauw, J.; Jacquet, D.; Le Beyec, Y.; Chaumont, J.; Bernas, H. *Phys. Rev. Lett.* **1998**, *80*, 5433.
- (56) Sun, S.; Szakal, C.; Winograd, N.; Wucher, A. Unpublished material.
- (57) Sigmund, P. In *Sputtering by Particle Bombardment I*; Behrisch, R., Ed.; Topics in Applied Physics; Springer-Verlag: Berlin, NY, 1981; Vol. 47, p 9.
- (58) Postawa, Z.; Wucher, A.; Winograd, N.; Garrison, B. J. Unpublished material.
- (59) Andersen, H. H. *Mater. Fys. Meddel.* **1992**, *127*, and references therein.
- (60) Brizzorala, R. A.; Cooper, C. B. *Nucl. Instrum. Methods B* **1989**, *43*, 136.
- (61) Wahl, M.; Wucher, A. *Nucl. Instrum. Methods B* **2000**, *164*, 687.
- (62) Winograd, N. *Mater. Fys. Meddel.* **1992**, *223*, and references therein.
- (63) Toyoda, N.; Kitani, H.; Hagiwara, N.; Aoki, T.; Matsuo, J.; Yamada, I. *Mater. Chem. Phys.* **1998**, *54*, 262.